RSC Advances

ROYAL SOCIETY OF CHEMISTRY

www.rsc.org/advances

RSC Advances

PAPER

Synthesis and Enhanced Photoelectric Performance of Au/ZnO Hybrid Hollow Sphere

Received 00th January 20xx,
Accepted 00th January 20xx

DOI: 10.1039/x0xx00000x

www.rsc.org/

Qin Wang, Linfeng Hu, Min Chen* and Limin Wu

A series of Au/ZnO hybrid hollow-sphere films were successfully prepared by "hexane-water" interfacial self-assembly of polystyrene (PS)/Au/ZnO nanocomposite spheres as building blocks followed by annealing treatment, and then used to fabricate nanodevices. The morphology and structure of the PS/Au/ZnO nanospheres and the as-transformed Au/ZnO hybrid hollow spheres were characterized by TEM, SEM, HRTEM, XRD, etc. It was found that the maximum responsivity (R_λ) and photocurrent of Au NPs decorated ZnO hollow-sphere nanofilm based nanodevice in the study showed more than 10 times enhancement when illuminated by 340nm UV light, as compared with that of pure ZnO hollow spheres. Further results demonstrate that high performance of the Au/ZnO hybrid hollow-sphere film based devices are attributed to the strong absorption and scattering of incident light and improved interfacial charge separation owing to the unique structure of the building block.

1 Introduction

Monodisperse hollow spheres have attracted wide attention for their potential applications such as catalysis, fillers, drug release systems, photonic crystals, protection of biologically active agents, and waste removal over the past decades due to their well-defined morphology, uniform size, low density and high surface area.[1-4]

Recently, more and more researches in this area have been focused on constructing high performance nanodevices by using hollow spheres as building blocks.[5, 6] For instance, it has been found that gas sensors constructed from WO_3 hollow spheres exhibited high sensitivity to various organic gases.[7] Lithium battery anode based on hollow SnO_2 microspheres exhibited extraordinarily high discharge capacities and higher coulombic efficiency than the theoretical value.[8] We have also presented the first hollow-sphere nanofilm based photodetector using ZnO hollow spheres as building blocks by oil-water interfacial self-assembly strategy.[9] Moreover, we extended this approach to fabricate ZnS-, $SrTiO_3$-, and ZnO/ZnS bilayer- hollow-sphere nanofilm photodetectors, which displayed high sensitivity, good stability and fast response speed.[10-12] Also, to further increase the light-absorption efficiency of hollow spheres, Golberg and co-workers reported a bubble-mediated approach to fabricate ZnO hollow spheres with double-yolk egg structures (DEHs), to construct an UV photodetector.[13] It was found that the large surface-to-volume ratio of hollow structures can increase the exposure area to harvest lights and the number of surface trap state to extend the recombination of electrons and holes, thus improving the photoelectric performance of the corresponding nanodevices. Among these, ZnO seems to be one of the best candidates for UV detection[14-19] since it has a wide direct band gap (~3.37 eV at room temperature) with a large exciton binding energy of 60 meV.[20]

Very recently, it has been found that incorporation of noble metal nanoparticles can greatly improve the performance of ZnO in many different applications, such as photocatalysis, plasmon-enhanced spectroscopy, gas sensors, biotechnology, solar cells and photodetectors.[21-29] For example, hierarchical flower-like ZnO nanostructures functionalized by Au nanoparticles via electrodeposition, showed improved photocatalytic activity and high performance as Li-ion battery anodes.[28] Gogurla *et al.* successfully synthesized Au functionalized ZnO nanosheets for enhanced UV photodetector and room temperature nitric oxide (NO) sensing devices via a simple photoreduction method.[30] Jin *et al.* prepared high-performance flexible ultraviolet photoconductors based on solution-processed ultrathin Au/ZnO nanoparticle composite films with responsivity (R_λ) as high as 1.51×10^5 AW^{-1} and T of over 90%.[31] The reasons for the enhanced performance of Au/ZnO devices in comparison to pure ZnO may include two aspects: (1) the localized surface plasmon resonance (LSPR) of Au nanostructures arising from light induced collective oscillation of free electrons can result in strong absorption, and scattering of incident light. (2) Au nanostructures can act as a reservoir for photo-induced charge carriers, thereby promoting interfacial charge separation process.[32, 33] Nonetheless, little research involves in the effect of noble metal nanoparticles on the optoelectronic properties of hollow-sphere nanofilm based nanodevices reported to the best of our knowledge. It seems

Department of Materials Science and State Key Laboratory of Molecular Engineering of Polymers, Fudan University, Shanghai 200433, China. E-mail: chenmin@fudan.edu.cn

to be difficult to load and control the amount of Au nanoparticles on hollow-sphere samples, which would be desirable for the development of new-generation nanodevices.

In this study, we have successfully loaded Au nanoparticles into the interior surface of ZnO hollow spheres and further constructed their nanofilm photodetector by using the Au nanoparticles decorated ZnO (Au/ZnO) hybrid hollow spheres as the building blocks. Polystyrene spheres (PS, 230 nm) were coated by the pre-synthesized Au nanoparticles (Au NPs, 15 nm) through electrostatic interaction then Zn^{2+} ions by coordination of the amide groups, followed by treatment with NaOH solution to form well-defined PS/Au/ZnO core-shell nanospheres. These spheres were self-assembled at an oil-water interface to form a precursor film.[9-12] After annealing, an Au/ZnO hybrid hollow-sphere nanofilm and then its corresponding nanofilm-based nanodevice were fabricated followed by a deposition of Cr/Au electrodes via e-beam evaporation. This nanodevice displayed almost ten times photocurrent compared with that of the pure ZnO hollow sphere-nanofilm-based accompanies.

2 Experimental

2.1 Materials

Styrene (St, 99 %) obtained from Sinopharm Chemical Reagent Co., Ltd. (China) was purified with 5 wt. % aqueous NaOH solution to remove any inhibitors and dried over anhydrous calcium chloride before use. Poly (vinyl pyrrolidone) (PVP, MW: 55000 g·mol^{-1}) and 2, 2′-azobis (2-methylpropionamidine) dihydrochloride (AIBA) were supplied by Sigma-Aldrich (Shanghai). Ethanol, hexane, zinc acetate dihydrate ($Zn(Ac)_2 \cdot 2H_2O$), sodium hydroxide (NaOH), gold (III) chloride hydrate ($HAuCl_4 \cdot 4H_2O$) and sodium citrate dihydrate ($C_6H_5Na_3O_7 \cdot 2H_2O$) were purchased from Sinopharm Chemical Reagent Co., Ltd. (China). Deionized water (≈17 MΩ cm^{-1}) was used throughout the experiment.

2.2 Synthesis of Au Nanoparticles

Citrate-stabilized Au NPs were prepared as follows.[34] All glassware was cleaned thoroughly with aqua regia (HNO_3: HCl=1:3) and rinsed with deionized water. 50 mL of 1 mM $HAuCl_4$ aqueous solution was heated to boiling under constant vigorous stirring, and then added rapidly by 5 mL of 1 wt. % boiling sodium citrate. After 20 s, the mixture became dark and burgundy, and then kept at 100°C under stirring for another 10 min to form Au NPs dispersion. After cooled to room temperature, the obtained Au NPs were stored in a brown bottle and kept in refrigerator for further use.

2.3 Synthesis of Monodisperse PS Spheres

Monodisperse positively charged PS particles were synthesized by emulsion polymerization described as follows: St (9.2 mL), deionized water (90 mL), and PVP (1.60 g) were charged into a 250 mL four-neck flask equipped with a mechanical stirrer, thermometer with a temperature controller, an N_2 inlet, a Graham condenser and a heating mantle. The reaction solution was stirred constantly and degassed by nitrogen gas at room temperature for approximately 30 min, and then heated to 70 °C, followed by addition of AIBA (0.4 g of AIBA dissolved in 10 g of water). This reaction was conducted at 70 °C for another 10 h, and then cooled to room temperature to obtain PS dispersion with 8.05 % solid content.

2.4 Adsorption of Au Nanoparticles onto PS Spheres

The as-prepared PS dispersion (0.52 g) was centrifuged at 15000 rpm for 30 min from the reaction medium and then dispersed homogeneously in 40 mL of water, followed by dropwise addition of various amounts of Au NPs. The resultant mixture was kept under gently stirring overnight. After that, Au NPs decorated PS spheres were transferred from water to ethanol for subsequent reaction via several centrifugation-redispersion cycles with a moderate amount of ethanol.

2.5 Preparation of PS/Au/ZnO Hybrid Core-shell Spheres

The above Au NPs decorated PS sphere dispersion was mixed with 30 g of $Zn(Ac)_2.2H_2O$ ethanol solution (0.6 wt. %) and stirred at 60 °C for 1 h, then dropped by 20 g of NaOH ethanol solution (0.31 wt. %) within 2 h, and stirred at 60 °C for another 1 h to obtain PS/Au/ZnO core-shell spheres, as shown in **Scheme 1**. The as-obtained hybrid sphere suspensions were purified by centrifugation-redispersion cycles for several times, and redispersed into 10 g of deionized water.

2.6 Fabrication of PS/Au/ZnO sphere based nanofilm

The hybrid core-shell sphere based nanofilms were fabricated by a "hexane-water" interfacial self-assembly method using the following procedure: [35] Firstly 2 g of the as-prepared PS/Au/ZnO suspension was diluted with 40 mL of deionized water. Then hexane (6 mL) was added into the top surface of the above dispersion to form a "hexane-water" interface. After that, ethanol as the inducer, was slowly added by a syringe to the interface at a relatively low rate (4 mL/h), during which the hybrid spheres were gradually gathered at the hexane-water interface to construct a densely packed film. After most of the hexane was removed carefully, the as-obtained film was transferred onto a thermally oxidized Si substrate covered with a 200 nm SiO_2 layer by pulling the substrate out of the liquid phase slowly. Repeat the above procedure once more to achieve bilayer films.

2.7 Fabrication of UV photodetectors

The as-assembled nanofilm was further calcined in air from room temperature to 600 °C at a heating rate of 1 °C min^{-1} and maintained at 350 and 600 °C for 2 h, respectively, to obtain

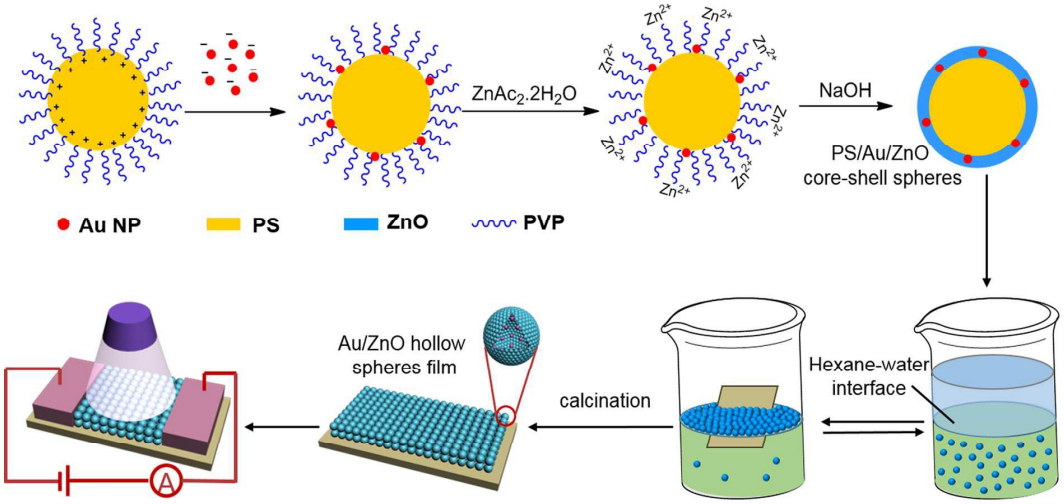

Scheme 1. Schematic illustration for the preparation of PS/Au/ZnO hybrid core-shell spheres and the fabrication of Au/ZnO hybrid hollow sphere based nanofilm and its device

Au/ZnO hybrid hollow-sphere based nanofilm. Afterwards the as-transformed nanofilm was transported to an E-beam evaporation system (LAB18) for deposition of the Cr/Au (10 nm/100 nm) electrodes.

2.8 Characterization

The morphologies of the products were observed by a transmission electron microscope (TEM, Tecnai G2 20 TWIN) and a field-emission scanning microscope (FESEM, Ultra 55). The chemical composition and elemental distribution were characterized by the high-resolution TEM (HRTEM, Philips XL30 HRTEM) and energy-dispersive X-ray spectroscopy (EDS) at an acceleration voltage of 200 kV. The phase components of the as-synthesized samples were determined by a Rigaku D/max-rB X-ray diffractometer using Cu Kα radiation (λ =0.15406 nm) with a scanning rate of 10 °/min and 2θ⍰ ranging from 20° to 80°. The UV-vis absorption spectra were scanned by a Hitachi U-4100 spectrophotometer. The Au/Zn molar ratios of the products were measured by an inductively coupled plasma atomic emission spectrometer (ICP-AES, P-4010). The samples were dissolved in 4:1 v/v HCl: HNO_3 (conc) and diluted with deionized water. The current-voltage (*I-V*) and time–dependent response (*I-t*) characteristics of these devices were measured using an Advantest Picoammeter R8340A and a dc voltage source R6144.

3 Results and discussion

The TEM and DLS results in **Fig. 1** indicate that the citrate capped Au NPs have an average diameter of 15 nm and negative charge surface of -38.3 mV. The dispersion showed an absorbance with maximum at 522 nm (Fig. 1c), consistent with previous work.[34, 36, and 37] **Fig. 2** shows the positively charged PS 230 nm in mean diameter, as well as raspberry-like PS/Au hybrid spheres with various amounts of Au nanoparticles. After Zn^{2+} ions were adsorbed onto the surfaces of PVP-stabilized PS spheres via coordination of the amide groups, and treated by NaOH solution and heated, PS/Au/ZnO core-shell spheres with average diameter of around 280 nm and shell thickness of 25 nm were obtained, as shown in **Fig. 2**. With increasing Au NPs on the PS surfaces, the core-shell morphology was kept. But too many Au NPs could cause free ZnO particles in the system owing to the steric hindrance of Au NPs.

Fig. 3a shows the UV-vis absorption of PS/Au/ZnO dispersions with various amounts of Au NPs. The peak at around 350 nm exhibits well-defined exciton band of ZnO, and the absorption band at around 522 nm appears for all the PS/Au/ZnO hybrid core- shell spheres, which is attributed to the LSPR effect of Au NPs.[38] As the amount of Au NPs embedded in the spheres increases, the absorption intensity around 520 nm increases significantly, and the corresponding colors of the dispersions change gradually from white, pink, purple to deep red, which indicates an increased coupling of plasmon resonances of adjacent gold nanoparticles.[39] Compared with the plasmon resonance absorption of pure Au dispersion, there is an obvious red-shift and broadening for

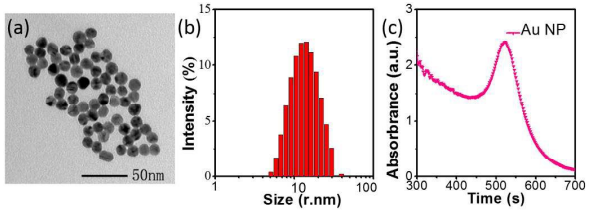

Fig. 1 (a) TEM image of Au NPs with an average diameter of 15nm; (b) the histogram of the size distribution of the resulting Au NPs, analyzed by DLS; (c) The UV-vis absorption spectrum of Au NPs solution.

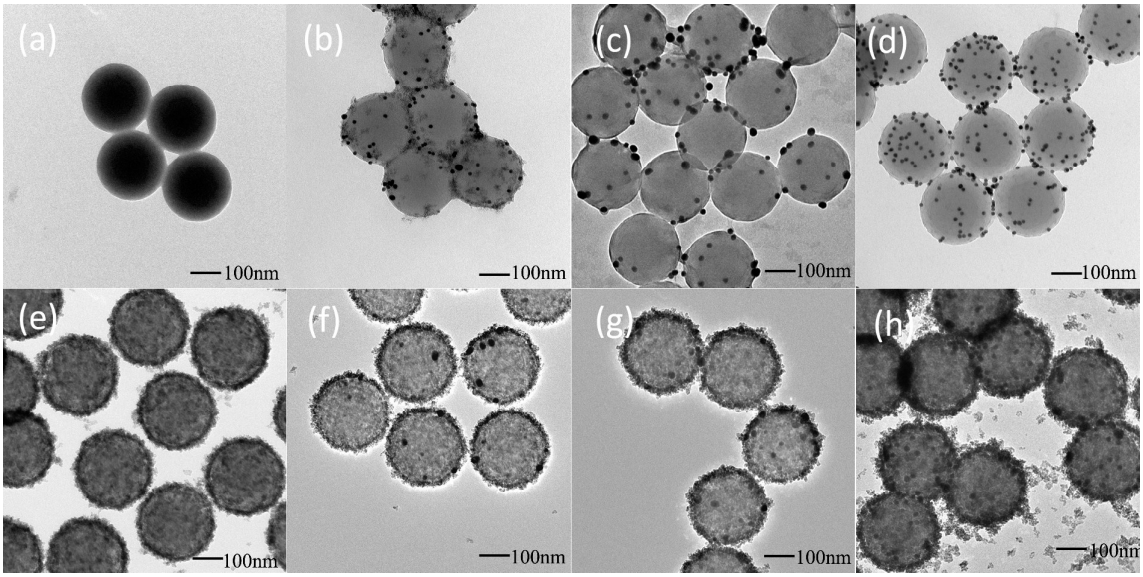

Fig. 2 TEM images of (a) PS and PS/Au hybrid spheres with molar additions of Au NPs (b) 1×10^{-5} mol, (c)2.5×10^{-5} mol, and (d) 4×10^{-5} mol, respectively. TEM images of (e) PS/ZnO and PS/Au/ZnO hybrid core-shell spheres with molar ratios of Au: ZnO (f) 0.012:1, (g) 0.030:1, and (h) 0.048:1 in reactants, respectively.

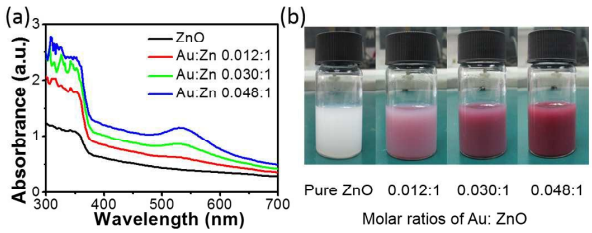

Fig. 3 (a) UV-vis absorption spectra of PS/Au/ZnO dispersions with various molar ratios of Au: ZnO; (b) The corresponding photographs of the samples.

PS/Au/ZnO spheres, which should be attributed to inter-particle coupling due to the dipole-dipole interaction between adjacent nanoparticles. It's clear that as the increase of Au NPs embedded, the distance between every two Au NPs decreases. [40] On the other hand, the LSPR of Au NPs gives rise to a significantly enhanced local electromagnetic field in the near-field region close to the Au NPs surface, which can efficiently increase the light absorption of the products throughout the wavelength range from 300 to 700 nm. [21]

Fig. 4 displays the typical SEM images of the nanofilms with different Au contents, from which one can see a series of closely packed continuous Au/ZnO hybrid hollow sphere nanofilms. Some spheres are broken probably because of gas release during calcination.

The XRD pattern for the pure ZnO in **Fig. 5a** displays all the diffraction peaks to hexagonal wurtzite ZnO phase (JCPDS 36-1451) without any peaks of impurities. For the Au-decorated ZnO, it can be seen that the peaks, (110), (200), (220), (311) planes of Au start to emerge and their intensities gradually increase with the increase of Au/Zn molar ratios in the reactants. The typical HRTEM image of as-prepared hybrid hollow sphere (mole ratio of Au: Zn was 0.048:1) indicates the d spacings of 0.24, 0.20, 0.25 and 0.28 nm (**Fig. 5b-c**), corresponding well with the (111) and (200) planes of Au nanoparticles and the (101) and (100) planes of ZnO particles, respectively. The TEM elemental mappings as shown in **Fig. 5d-g**, indicate that Zn and O are homogeneously distributed within each individual sphere, while Au NPs are indeed located at the interior surface of ZnO hollow sphere.

The actual Au/Zn molar ratios in products measured by ICP-AES are 0, 0.025:1, 0.034:1, and 0.067:1, respectively, which are higher than their initial feed ratios. This is probably due to the existence of some free ZnO particles, which was removed by the centrifugation process.

Fig. 6a-e demonstrates the typical SEM image of Au/ZnO hybrid hollow spheres film- based nanodevice and the current-voltage (*I-V*) curves when the nanofilm-devices with various Au/Zn ratios illuminated under different lights. The linear behavior of the photocurrent curve indicates Ohmic contact between hollow spheres and the Cr/Au electrodes. The photocurrent of all the devices show very slight changes when the wavelengths of the light source are 600 nm (1.16 mW·cm^{-2}), 500 nm (2.30 mW·cm^{-2}) and 400 nm (2.37 mW·cm$^{-2)}$, and the dark current is also extremely low. An abrupt increase of photocurrent is observed when the device is illuminated by 370 nm (2.12 mW·cm^{-2}) and 340 nm (1.63 mW·cm^{-2}) UV lights, which suggests that the device is highly UV-sensitive. From the response time of the photodetectors measured at 5V illuminated by light of 340 nm, as shown in **Fig. 6f**, it can be clearly seen that with the increase of Au NPs in the hollow spheres, the photocurrent of device reveals a drastic enhancement. Especially, the photocurrent of Au/ZnO (Au: Zn=0.048:1) based device is almost 10 times that of control

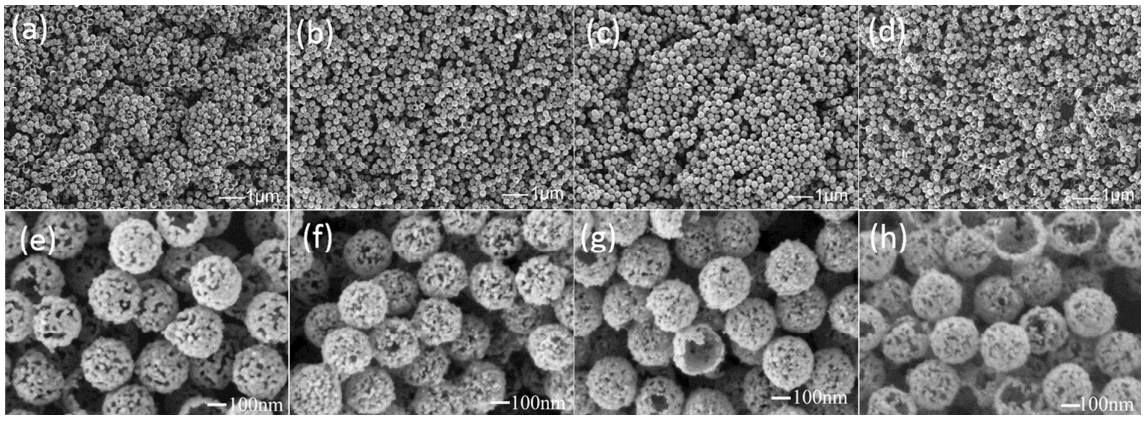

Fig.4. SEM images of Au/ZnO hybrid hollow-sphere based nanofilms with different Au/Zn molar ratios of 0, 0.012, 0.030, and 0.048 in reactants at (a), (b), (c), (d) low and (e), (f), (g), (h) high magnification.

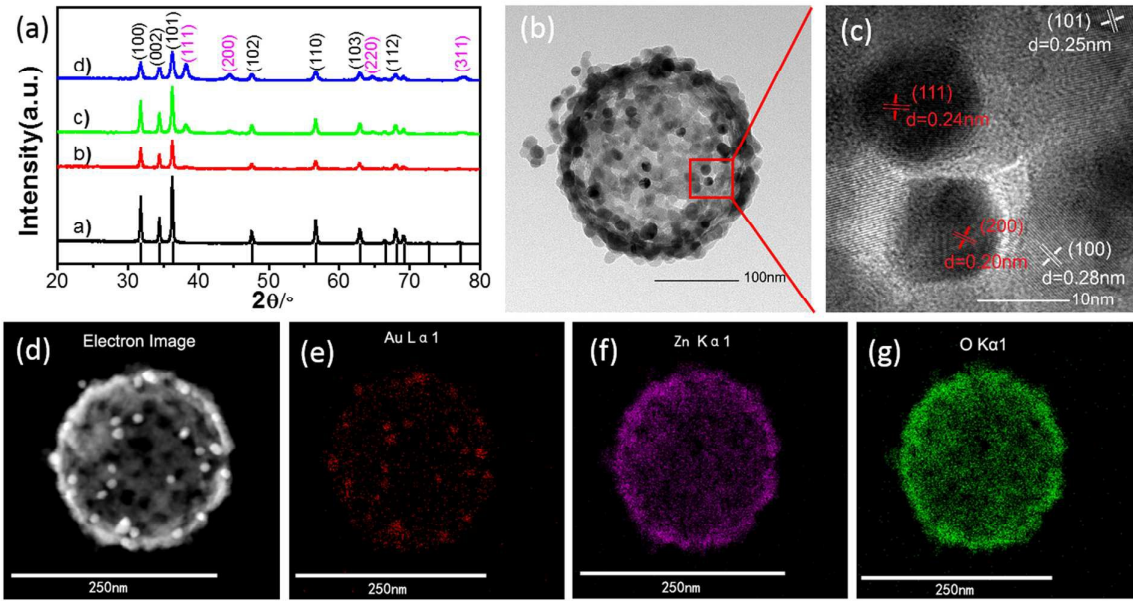

Fig. 5 (a) XRD patterns of Au/ZnO powders with different Au/Zn molar ratios a) 0, b) 0.012, c) 0.030, d) 0.048 in reactants; (b)TEM , (c)HRTEM and (d)Electron image images of single Au/ZnO hybrid hollow sphere; (e), (f) and (g) Au, Zn and O elemental maps, respectively.

ZnO hollow sphere nanofilm counterpart which has exhibited significantly enhanced photoelectric performance than ZnO nanowire-based nanodevices.[9, 12]

The responsivity (R_λ), defined as the photocurrent per unit of incident optical power and the external quantum efficiency (*EQE*), defined as the number of electrons detected per incident photon can be calculated as the following equations respectively.

$$R_\lambda = \frac{\Delta I}{PA}$$

$$EQE = \frac{hc}{e\lambda} R_\lambda$$

Where ΔI is the difference between the photo-excited current and the dark current, P is the power density irradiated on the sample and A is the irradiated area of the device, λ is the exciting wavelength, h is Planck's constant, c is the velocity of the light, and e is the electronic charge.[41] As shown in **Table 1**, as more Au NPs embedded, both R_λ and *EQE* increase. The R_λ and *EQE* of Au/ZnO hybrid hollow sphere nanofilm-based device (Au: Zn=0.048:1) are 106.3 A·W^{-1} and 38842% at 340 nm at a bias of 5 V respectively, which are also almost of ten times of ZnO hollow spheres (about 10.6 A·W^{-1} and 3873%, respectively). The greatly enhanced photocurrent and

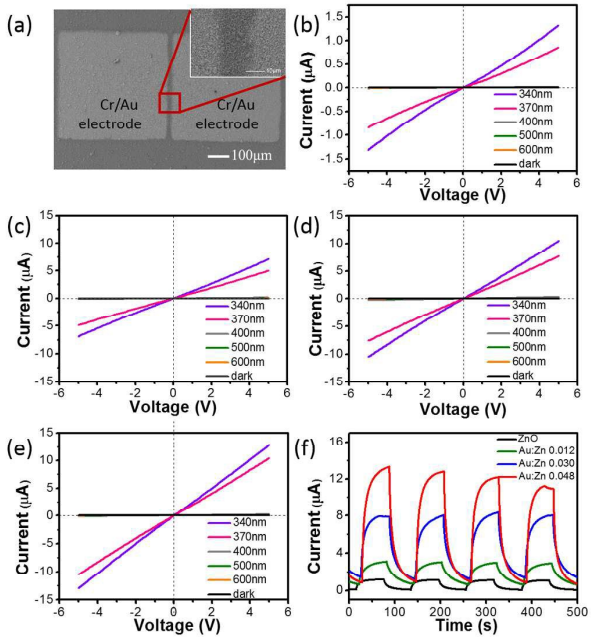

Fig. 6 (a) SEM images of hollow-sphere film device; I-V characteristics of the devices constructed from (b) ZnO and (c)-(e) Au/ZnO (with various Au: Zn ratios 0.012, 0.030, 0.048) nanofilms illuminated by light of 340 nm, 370 nm, 400 nm, 500 nm, 600 nm and under dark conditions; (f) Response times of the photodetectors measured in air at a bias of 5.0 V illuminated by light of 340 nm.

photocurrent to dark current ratio suggests that Au NPs have great advantages in improving the performance of ZnO hollow sphere-based nanodevices. Compared with the individual nanowire based photodetectors (photocurrent of 0.65μA for Au/ZnO nanowire at 1V [32] and 5.21nA for Ag/ZnO nanowire at -0.5V [33]), high photocurrent of the present nanofilm device might be ascribed to a fact that the photocurrent of the device is collected from a large number of Au/ZnO hybrid hollow spheres rather than a single one. Such a drastic enhancement is very promising for practical application such as field emitters, light emission diodes (LEDs), photodiodes, etc. Furthermore, as shown in Table 1, the present device exhibits a higher I_l/I_d and larger R in comparison with that of Au/ZnO nanosheet based photodetector (I_l/I_d=1923 and R=0.05AW^{-1} at 5V, respectively).[30]

Two main mechanisms are possibly contributed to the photoresponse of the devices.[42, 43] One is the fast generation of electron-hole pairs in ZnO, and the other is a hole-trapping

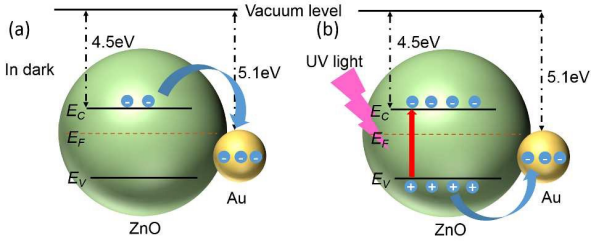

Scheme 2. The schematics of the energy level diagrams of Au/ZnO hybrid hollow spheres and the charge transfer process in dark (a) and under UV light illumination (b).

mechanism by the chemisorbed O_2^- ions on the surface of hollow spheres. In the dark condition, the O_2 adsorbed onto the hollow-sphere surface can capture free electrons from n-type ZnO [$O_{2\,(g)} + e^- \rightarrow O_{2\,(ad)}^-$], creating a depletion layer with low conductivity near the surface. Under UV illumination, electron-hole pairs are generated [$h\nu \rightarrow h^+ + e^-$] since the photon energy is above the threshold excitation energy of ZnO. The photogenerated holes migrate to the surface along the potential gradient and are trapped by O_2^-, inducing the desorption of oxygen from the ZnO surface [$h^+ + O_{2\,(ad)}^- \rightarrow O_{2\,(g)}$]. The photogenerated electrons are collected by the anode, and a decrease in the width of the depletion resulted in a drastic increase of photocurrent.[9]

Since the work function of Au (φ_{Au}=5.1eV) is larger than that of ZnO (φ_{ZnO}=4.5eV), electrons will transfer from the conduction band of n-ZnO to Au, forming a Schottky barrier at the interface, until Au NPs and ZnO have the same Fermi energy level (E_F), as shown in **Scheme 2a**. When the Au-decorated ZnO hollow sphere based device is illuminated by UV light, the photogenerated holes not only recombine owing to O_2^- ions, but also pass through the Schottky interface to Au NPs due to the built-in potential and electron-hole recombination, thereby decreasing the width of the depletion layer. In addition, the hole-trapping of the Schottky barrier at the Au-ZnO interface allows for more electrons to be collected by electrodes, as shown in Scheme 2b.[32, 33] In short, after light absorption and the formation of an exciton in ZnO region, the negatively charged Au NPs can trap the photo-induced charge carriers, and therefore promote the charge separation and improve the photocurrent. And as evidenced in **Fig.4a**, the effect of LSPRs arising from Au NPs can cause a strong absorption, scattering and local field enhancement, therefore increasing the absorption of photons.[30]

Table 1. Comparison of the critical parameters for ZnO hollow spheres with different Au contents based UV devices

Au : Zn molar ratios	Light of detection	Bias/V	Dark current/I_d	Photocurrent/I_l	I_l/I_d	R_λ/AW^{-1}	EQE
0:1	340nm	5	0.24nA	1.29μA	5375	10.6	3873%
0.012:1	340nm	5	1.54nA	6.89μA	4474	56.4	20609%
0.030:1	340nm	5	0.47nA	10.5μA	22340	85.9	31388%
0.048:1	340nm	5	0.44nA	13.0μA	29545	106.3	38842%

4 CONCLUSION

In summary, we have successfully synthesized Au/ZnO hybrid hollow spheres and further fabricated these hollow spheres nanofilm-based nanodevices through "hexane-water" interfacial self-assembly strategy. The Au/ZnO hybrid hollow-spheres nanodevice exhibits significantly enhanced photocurrent, and relatively larger photocurrent to dark current ratio than pure ZnO hollow spheres nanofilm nanodevice. And the more the Au NPs embedded, the better the photoelectric performances are. When the molar ratio of Au/Zn at 0.048:1, the photocurrent of this Au/ZnO hybrid hollow-spheres nanofilm based photodetector shows as high as ten fold that of pure ZnO hollow nanofilm nanodevice. This dramatic enhanced photoelectric performances are attributed to the stronger UV absorption and hole-trapping by the negatively Au NPs. This method and the exciting results suggest that one can improve the photoelectric properties of semiconducting nanodevices by embedded or doped noble metals.

Acknowledgements

Financial supports of this research from the National Natural Science Foundation of China (51322307, 51273218, 51133001, 51372040 and 21374018), National "863" Foundation (2013AA031801), Science and Technology Foundation of Ministry of Education of China (20110071130002), Science and Technology Foundation of Shanghai (13JC1407800), and "Shu Guang" project supported by Shanghai Municipal Education Commission and Shanghai Education Development Foundation are appreciated.

Notes and references

1. F. Caruso, R. A. Caruso and H. Mohwald, *Science*, 1998, **282**, 1111-1114.
2. S. Kidambi, J. H. Dai, J. Li and M. L. Bruening, *J. Am. Chem. Soc.*, 2004, **126**, 2658-2659.
3. Y. L. Wang, L. Cai and Y. N. Xia, *Adv. Mater.*, 2005, **17**, 473-477.
4. L. Y. Wang and Y. D. Li, *Small*, 2007, **3**, 1218-1221.
5. M. Chen, C. Y. Ye, S. X. Zhou and L. M. Wu, *Adv. Mater.*, 2013, **25**, 5343-5351.
6. J. Zhang, S. R. Wang, Y. M. Wang, Y. Wang, B. L. Zhu, H. J. Xia, X. Z. Guo, S. M. Zhang, W. P. Huang and S. H. Wu, *Sens. Actuator B-Chem.*, 2009, **135**, 610-617.
7. X. L. Li, T. J. Lou, X. M. Sun and Y. D. Li, *Inorg. Chem.*, 2004, **43**, 5442-5449.
8. S. J. Han, B. C. Jang, T. Kim, S. M. Oh and T. Hyeon, *Adv. Funct. Mater.*, 2005, **15**, 1845-1850.
9. M. Chen, L. F. Hu, J. X. Xu, M. Y. Liao, L. M. Wu and X. S. Fang, *Small*, 2011, **7**, 2449-2453.
10. W. Z. Shan, L. F. Hu, X. Lin, M. Chen and L. M. Wu, *J. Mater. Chem.*, 2012, **22**, 17671-17676.
11. C. Y. Ye, J. X. Xu, S. X. Zhou, M. Chen and L. M. Wu, *Langmuir*, 2013, **29**, 13502-13508.12.
12. L. F. Hu, M. Chen, W. Z. Shan, T. R. Zhan, M. Y. Liao, X. S. Fang, X. H. Hu and L. M. Wu, *Adv. Mater.*, 2012, **24**, 5872-5877.
13. X. Wang, M. Y. Liao, Y. T. Zhong, J. Y. Zheng, W. Tian, T. Y. Zhai, C. Y. Zhi, Y. Ma, J. N. A. Yao, Y. Bando D. Golberg, Adv. Mater., 2012, 24, 3421-3425.
14. Z. Alaie, S. M. Nejad and M. H. Yousefi, *Mater. Sci. Semicond. Process*, 2015, **29**, 16-55.
15. J. Zhou, Y. D. Gu, Y. F. Hu, W. J. Mai, P. H. Yeh, G. Bao, A. K. Sood, D. L. Polla and Z. L. Wang, *Appl. Phys. Lett.*, 2009, **94**.
16. E. Monroy, F. Omnes and F. Calle, *Semicond. Sci. Technol.*, 2003, **18**, R33-R51.
17. T. Y. Zhai, X. S. Fang, M. Y. Liao, X. J. Xu, H. B. Zeng, B. Yoshio and D. Golberg, *Sensors*, 2009, **9**, 6504-6529.
18. C. H. Lin and C. W. Liu, *Sensors*, 2010, **10**, 8797-8826.
19. K. W. Liu, M. Sakurai and M. Aono, *Sensors*, 2010, **10**, 8604-8634.
20. H. Kind, H. Q. Yan, B. Messer, M. Law and P. D. Yang, *Adv. Mater.*, 2002, **14**, 158-160.
21. R. B. Jiang, B. X. Li, C. H. Fang and J. F. Wang, *Adv. Mater.*, 2014, **26**, 5274-5309.
22. L. P. Liu, H. T. Yang, X. Ren, J. Tang, Y. F. Li, X. Q. Zhang and Z. H. Cheng, *Nanoscale*, 2015, **7**, 5147-5151.
23. L. W. Wang, S. R. Wang, H. X. Zhang, Y. S. Wang, J. D. Yang and W. P. Huang, *New J. Chem.*, 2014, **38**, 2530-2537.
24. X. M. Hou and L. X. Wang, *RSC Adv.*, 2014, **4**, 56945-56951.
25. L. L. Wang, Z. Lou, T. Fei and T. Zhang, *J. Mater. Chem.*, 2012, **22**, 4767-4771.
26. H. T. Ding, J. Y. Shao, Y. C. Ding, W. Y. Liu, H. M. Tian and X. M. Li, *ACS Appl. Mater. Interfaces*, 2015, **7**, 12713-12718.
27. J. D. Hwang, F. H. Wang, C. Y. Kung and M. C. Chan, *IEEE Trans. Nanotechnol.*, 2015, **14**, 318-321.
28. M. Ahmad, Y. Y. Shi, A. Nisar, H. Y. Sun, W. C. Shen, M. Wei and J. Zhu, *J. Mater. Chem.*, 2011, **21**, 7723-7729.
29. X. W. Li, W. Feng, Y. Xiao, P. Sun, X. L. Hu, K. Shimanoe, G. Y. Lu and N. Yamazoe, *RSC Adv.*, 2014, **4**, 28005-28010.
30. N. Gogurla, A. K. Sinha, S. Santra, S. Manna and S. K. Ray, *Sci Rep*, 2014, **4**. 6483
31. Z. W. Jin, L. Gao, Q. Zhou and J. Z. Wang, *Sci Rep*, 2014, **4**. 4268
32. K. W. Liu, M. Sakurai, M. Y. Liao and M. Aono, *J. Phys. Chem. C*, 2010, **114**, 19835-19839.
33. S. K. Tzeng, M. H. Hon and I. C. Leu, *J. Electrochem. Soc.*, 2012, **159**, H440-H443.
34. D. M. Dotzauer, J. H. Dai, L. Sun and M. L. Bruening, *Nano Lett.*, 2006, **6**, 2268-2272.
35. L. F. Hu, M. Chen, X. S. Fang and L. M. Wu, *Chem. Soc. Rev.*, 2012, **41**, 1350-1362.
36. P. F. Guo, J. Y. Xu, X. J. Zhuang, W. Hu, X. L. Zhu, H. Zhou, L. J. Tang and A. L. Pan, *J. Mater. Chem. C*, 2013, **1**, 566-571.
37. H. B. Xia, S. O. Bai, J. Hartmann and D. Y. Wang, *Langmuir*, 2010, **26**, 3585-3589.
38. Y. C. Liu, M. Y. Zhong, G. Y. Shan, Y. J. Li, B. Q. Huang and G. L. Yang, *J. Phys. Chem. B*, 2008, **112**, 6484-6489.
39. H. Ko, S. Chang and V. V. Tsukruk, ACS Nano, 2009, 3, 181-188.

40. Y. J. Chen, G. H. Tian, K. Pan, C. G. Tian, J. Zhou, W. Zhou, Z. Y. Ren and H. G. Fu, *Dalton Trans.*, 2012, **41**, 1020-1026.
41. X. S. Fang, L. F. Hu, K. F. Huo, B. Gao, L. J. Zhao, M. Y. Liao, P. K. Chu, Y. Bando and D. Golberg, *Adv. Funct. Mater.*, 2011, **21**, 3907-3915.
42. C. Soci, A. Zhang, B. Xiang, S. A. Dayeh, D. P. R. Aplin, J. Park, X. Y. Bao, Y. H. Lo and D. Wang, *Nano Lett.*, 2007, **7**, 1003-1009.
43. Y. Z. Jin, J. P. Wang, B. Q. Sun, J. C. Blakesley and N. C. Greenham, *Nano Lett.*, 2008, **8**, 1649-1653.

Table of contents entry

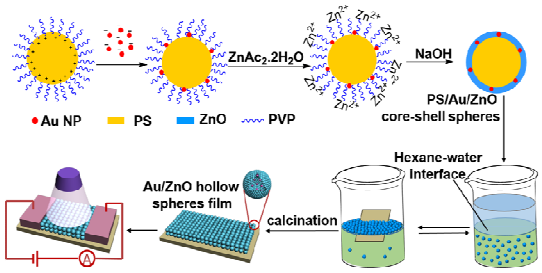

The maximum responsivity (R_λ) and photocurrent of Au/ZnO nanodevice showed 10 times enhancement than that of pure ZnO hollow spheres.